ACS OMEGA

http://pubs.acs.org/journal/acsodf

Article

Preparation of N,P Co-doped Porous Carbon Derived from Daylily for Supercapacitor Applications

Tianxiang Jin,* Jingwei Su, Qingyun Luo, Wei Zhu, Haizhen Lai, Dejuan Huang, and Chunyan Wang*

Cite This: *ACS Omega* 2022, 7, 37564−37571

Read Online

ACCESS | Metrics & More | Article Recommendations | Supporting Information

ABSTRACT: Biomass-derived activated carbon is a widely used electrode material for supercapacitors. One of the keys to preparing high-performance activated carbon is the selection of appropriate precursors. Daylily is a common edible herb and is widely planted in Asia. It is rich in nitrogen and phosphorus, so it can be used as a precursor of heteroatom-doped activated carbon. Herein, a daylily-derived porous carbon with a large specific surface area and high content of heteroatoms has been successfully prepared by a simple carbonization method. The as-prepared carbon materials showed a remarkable specific capacitance of 299.1 F/g at 0.5 A/g and excellent cycling stability of 99.6% after 4000 cycles at a current density of 1 A/g. Moreover, the assembled symmetric supercapacitor showed a high energy density of 21.6 Wh/kg at a power density of 598.2 W/kg in 6 M KOH electrolyte. These results demonstrate that the daylily-derived porous carbon is an excellent material for high-performance supercapacitors.

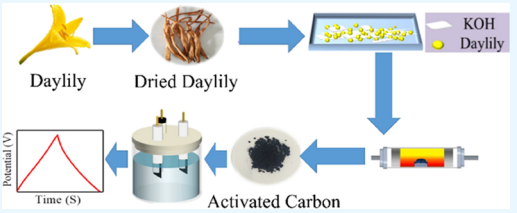

1. INTRODUCTION

Nowadays, the consumption of fossil fuels has been dramatically increased with the rapid development of global industrialization.[1] Energy storage has become one of the great challenges for mankind.[2] Therefore, the research related to high-performance and renewable energy storage components has attracted the interest of both researchers and manufacturers.[3−6] Supercapacitors are a widely used energy storage device. Because of their high power density, rapid charge and discharge rate, prolonged cycle life, and excellent stability,[7] supercapacitors have been used in many fields, such as power grids, high-power hybrid electric vehicles, and other ecofriendly energy applications.[8]

Based on the charge storage mechanism, supercapacitors can be divided into two categories: one is the electrical double-layer capacitor (EDLC) in which the capacitance arises from the charge separation at the electrode/electrolyte interface; the other is the pseudocapacitors associated with faradaic reactions of the electroactive species on the surface of the electrode.[9] Carbon materials are often used as electrode materials for supercapacitors due to their outstanding properties, such as good electrical conductivity, high surface area, and remarkable corrosion resistance.[10] Activated carbons (ACs),[11] carbon nanotubes (CNTs),[12] graphene,[13] and activated carbon fibers (ACFs)[14] are the most widely used carbon materials in supercapacitors. However, these materials are expensive and usually prepared from nonrenewable resources. In addition, most carbon-based supercapacitors are EDLCs. Therefore, their energy densities are generally lower than those of pseudocapacitors, which limit their further application.[15]

Incorporating heteroatoms into carbon frameworks is an effective way to solve the above problems. Heteroatoms can not only improve the specific capacitance of materials through the Faraday reaction, but also improve the conductivity and wettability of materials, which can significantly enhance the energy storage performance of supercapacitors.[16−21] For example, it is reported that the N-doping structure can increase the specific capacitance and electrical conductivity of carbon materials while P-doping atoms can enlarge the interlayer spacing of graphitic structures and offer more active sites for the reversible redox reaction.[22,23]

In recent years, based on the characteristics of low cost, easy availability, renewability, and environmental friendliness, biomass-derived porous carbon materials have attracted wide attention.[24] Their inherent chemical composition and biological geometries can be used as templates to manufacture electrode materials with a controllable chemical composition and well-defined porous structure.

Daylily (*Hemerocallis* sp.) is a common edible plant in China. It is rich in amino acids and lecithin, which can provide abundant nitrogen and phosphorus atoms for heteroatom-doped activated carbon, respectively. Therefore, we speculate that daylily may be a potential precursor of high-performance carbon electrode materials.

Based on the above analysis, in this paper, daylily-based porous activated carbon was prepared by a facile one-step

Received: July 11, 2022
Accepted: September 28, 2022
Published: October 13, 2022

https://doi.org/10.1021/acsomega.2c04369
ACS Omega 2022, 7, 37564−37571

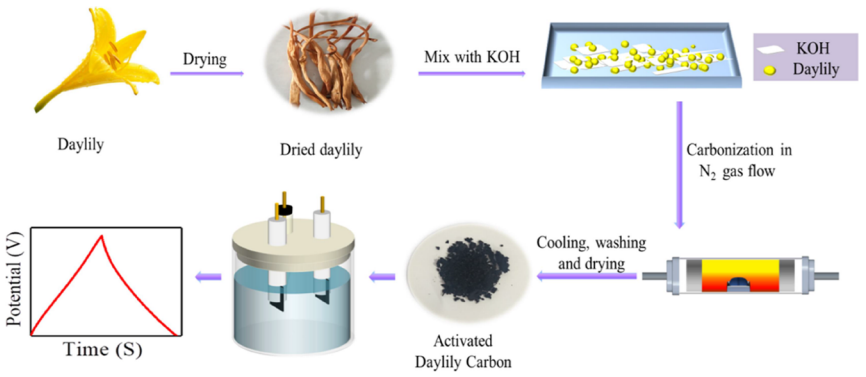

Figure 1. Schematic illustration of the synthesis and characterization of DAC samples.

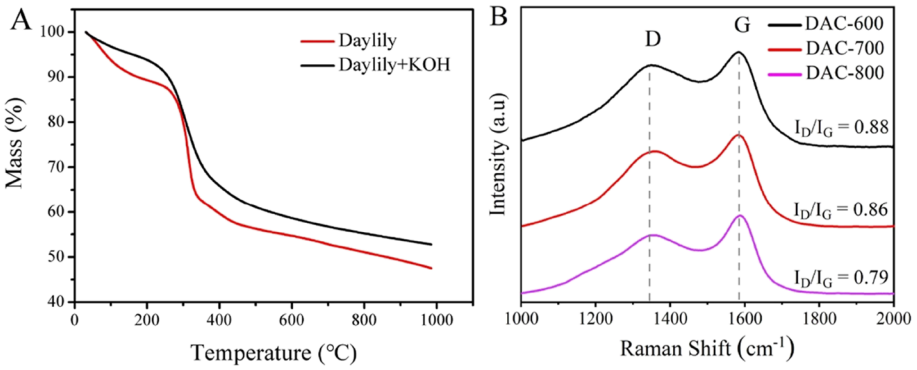

Figure 2. (A) TGA curves of raw daylily and the mixture of daylily and KOH with the weight ratio of 1:1. (B) Raman spectra of DAC samples.

carbonization process and used as an electrode material for supercapacitors. The electrochemical properties of daylily-based carbon were characterized comprehensively. The results manifest that the as-obtained carbon has reasonable nitrogen and phosphorus contents and exhibits a large specific surface area with a hierarchical pore structure. These features permit this N,P-codoped porous carbon material to show remarkable specific capacitance and excellent cycle durability. In addition, the as-fabricated supercapacitor also exhibited a high energy density, which further reflects its potential value for energy storage (Figure 1).

2. EXPERIMENT

2.1. Experiment Materials. The flowers of daylilies were purchased from the local market (Nanchang City, Jiangxi Province, China). Potassium hydroxide (KOH), sodium sulfate (Na_2SO_4), and hydrochloric acid (HCl) were obtained from Shanghai Aladdin Biochemical Technology Co., Ltd. Deionized water (DI) of high purity was used in this work. All reagents were of analytical purity and were not further purified.

2.2. Synthesis of Porous Carbon Materials. After freeze-drying, the daylilies were rolled into powder and mixed with KOH (the mass ratio of daylily and KOH was 1:2). Then, they were put into a tubular furnace, heated to 400 °C at 5 °C/ min in a nitrogen environment and kept for 1 h. Subsequently, the precarbonization products were heated to the targeted carbonization temperatures (600, 700, and 800 °C) at 5 °C/min and held for 2 h. The cooled product was cleaned with 1 mol/L HCl and deionized water three times, respectively. After drying for 12 h, the as-prepared carbon materials were marked as DAC-x (x is the value of carbonization temperature, x = 600, 700, and 800).

2.3. Material Characterization. The microstructure and morphology of the samples were observed by scanning electron microscopy (SEM) (FE-SEM, Hitachi S-4800). X-ray photoelectron spectroscopy (XPS) tests were performed via a Thermo Fisher X-ray photoelectron spectrometer equipped with Al radiation as the probe (Kα, radiation). X-ray diffraction (XRD) tests were carried out on an X-ray diffractometer (Bruker D8-A25). The nitrogen adsorption/desorption tests were performed via an Autosorb-iQ2-MP (Quantachrome) analyzer. Raman spectra were recorded on a Raman spectrometer (Thermo DXR, USA) using a 532 nm laser source. Thermogravimetric (TG) analysis was conducted under a N_2 atmosphere and heated to 1000 °C by a Netzsch STA 409 instrument with a heating rate of 15 °C min^{-1}.

2.4. Electrochemical Measurements. A three-electrode system was used to investigate the electrochemical performance of the samples. The working electrodes were prepared by mixing the active material with polytetrafluoroethylene and carbon black in a weight ratio of 8:1:1. The mixture was pressed onto the surface of nickel foam (1 × 1 cm^2), then dried at 80°C for 12 h.

A Hg/HgO electrode was used as a reference electrode, a platinum plate electrode was chosen as a counter electrode, and 6 M KOH solution was used as an electrolyte.

All electrochemical properties of DACs were investigated on an electrochemical workstation (CHI660E, Chenhua Instruments Co. Ltd., China).

For the three-electrode cell, the specific capacitance (C, F/g) was calculated from the GCD curves by eq 1:

$$C = \frac{I\Delta t}{m\Delta V} \quad (1)$$

https://doi.org/10.1021/acsomega.2c04369
ACS Omega 2022, 7, 37564−37571

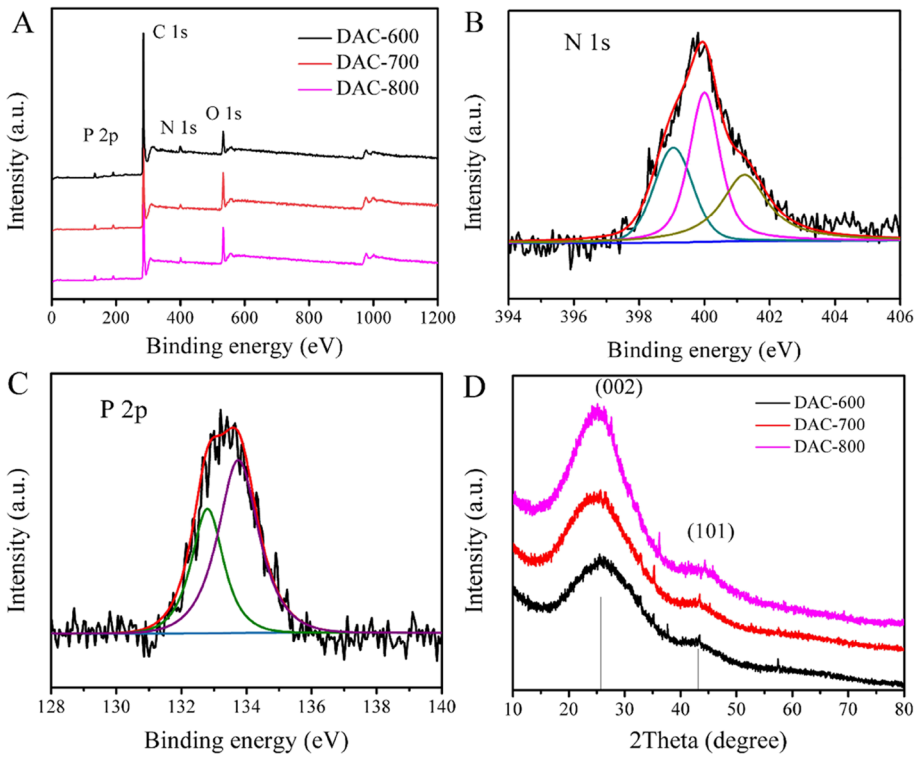

Figure 3. (A) XPS spectra of all DAC samples. High-resolution XPS spectrum of (B) N 1s and(C) P 2p for DAC-700. (D) XRD spectra of all DAC samples.

A two-electrode cell was also used to evaluate the practical application performance of electrode materials. The preparation process of the two-electrode cell is shown in Supporting Information S1. For this two-electrode cell, the specific capacitance (C, F/g) of a single electrode was obtained based on eq 2:

$$C = \frac{2I\Delta t}{m\Delta V} \tag{2}$$

In the symmetric system, the energy density (E, Wh/kg) and power density (P, kW/kg) were calculated by eq 3 and 4, respectively:

$$E = \frac{C\Delta V^2}{7.2} \tag{3}$$

$$P = \frac{3600E}{\Delta t} \tag{4}$$

where C (F/g) is the gravimetric specific capacitance of electrode materials, I (A) is the constant discharging current, Δt (s) is the discharge time, m (g) is the loading weight of DACs in a single electrode, and ΔV (V) is the voltage change in the discharge process.

3. RESULTS AND DISCUSSION

The TGA curves of both raw daylily and the mixture of KOH and raw daylily are shown in Figure 2A. Under 200 °C, the loss of weight is caused by the removal of the adsorbed water from KOH and daylily. At about 300 °C, the mixed sample exhibited a faster decomposition rate than raw daylily, which should be attributed to the etching effect of KOH. When the temperature is higher than 500 °C, the decomposition rates of these two samples were reduced evidently, indicating that stable structures of the carbon materials have already formed.

To further investigate the structures of DAC samples, Raman measurements were performed. As shown in Figure 2B, all DAC samples exhibited two broad peaks at about 1345 and 1586 cm^{-1}, corresponding to the D band and G band, respectively. The D band represents disordered (sp^3) carbon structures, and the G band is associated with graphitic (sp^2) carbon. The intensity ratios of D and G bands (I_D/I_G) can be used to evaluate the ordered and disordered nature of DACs.[25] The I_D/I_G ratio is 0.88, 0.86, and 0.79 for DAC-600, DAC-700, and DAC-800, respectively. This result indicates that the degree of graphitization of DACs increases with the carbonization temperature.

The chemical compositions of DAC samples were characterized via XPS. The XPS spectra in Figure 3A confirmed the existence of C, N, P, and O elements in all DAC samples. The contents of the heteroatoms are displayed in Table 1. As seen, the content of N decreased as the increasing of carbonization temperature, while the content of P did not decrease significantly. This phenomenon implies that the phosphorus-containing groups have a good chemical stability. The high-resolution XPS spectrum of N 1s is exhibited in Figure 3B. The

Table 1. Porous Structure Parameters and Element Contents of all Samples[a]

sample	elemental composition [at %] N	P	S_{BET} (m^2/g)	V_{Total} (cm^2/g)
DAC-600	4.9	3.8	834	0.58
DAC-700	4.3	4.1	1531	0.86
DAC-800	3.8	3.9	1279	0.77

[a] S_{BET}, the specific surface area; V_{Total}, the total volume.

https://doi.org/10.1021/acsomega.2c04369
ACS Omega 2022, 7, 37564−37571

deconvoluted N 1s curve has three peaks corresponding to pyridinic N (399.1 eV), pyrrolic N (400.0 eV) and quaternary N (401.2 eV), respectively.[26] According to literatures, the pyridinic N and pyrrolic N can not only provide additional pseudocapacitance through reversible faradaic reactions but also increase the wettability of carbon materials in aqueous electrolytes. In addition, the quaternary N can improve the electrical conductivity of carbon materials, which can further enhance the electrochemical performances of DAC electrodes.[27,28] In the high-resolution of P 2p spectra (Figure 3C), two peaks located at 132.8 and 133.7 eV represent C_3−P groups and C−O−P type groups, respectively.[29] Phosphorus has a relatively larger atomic radius compared to nitrogen and carbon. Therefore, the P atoms exhibiting the sp^3 configuration can form distortions and open edge structures to increase the active sites for energy storage. Furthermore, the abundant C−O−P groups can also improve the wettability and electrochemical stability of carbon materials.[22,30]

XRD test was carried out to explore the structure of DAC materials. As shown in Figure 3D, the XRD pattern exhibited two characteristic peaks at 2 theta values of 25.7° and 43.2° corresponding to the (002) and (101) crystalline planes of graphitic carbon, respectively.[31] Moreover, with the increase of carbonization temperature, the diffraction peak of DACs becomes narrower and intenser. This phenomenon indicates that DAC-800 and DAC-700 have a higher graphitization degree than DAC-600.

The morphology and microstructure of all DAC samples were observed by SEM. As shown in Figure 4A, DAC-600 exhibited

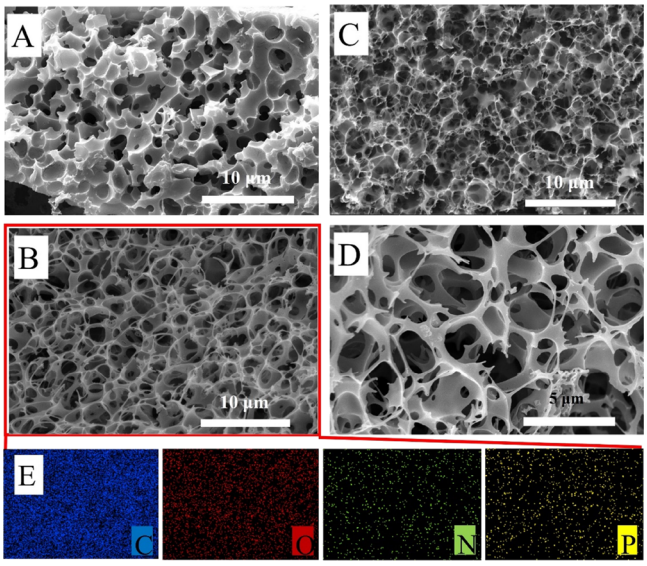

Figure 4. SEM images of (A) DAC-600, (B) DAC-700, (C) DAC-800, (D) DAC-700 at high magnification and (E) element mapping of DAC-700.

an incomplete porous structure. This may be due to the low carbonization temperature, which inhibited the activation of KOH. When the carbonization temperature reached 700 °C, the DAC-700 formed a well-developed three-dimensional porous network (Figure 4B). Figure 4D shows the SEM image of DAC-700 at a higher magnification. As seen, for DAC-700, the wall thickness of its carbon skeleton was about 0.1−0.2 μm. This phenomenon indicates that increasing the carbonization temperature is conducive to the formation of porous structure. However, it can be clearly observed from Figure 4C that there are a lot of fragmented structures in DAC-800. This should be attributed to the excessive corrosion at high temperatures, which led to the collapse of the porous structure. In addition, Figure 4D exhibited that oxygen, nitrogen, and phosphorus atoms are evenly distributed in DAC-700 samples.

Nitrogen adsorption/desorption isotherms were analyzed to investigate the pore structure of DAC samples. As shown in Figure 5A, the isotherms of all three samples show the typical IV isotherms. The steep platforms at low relative pressures indicate the existence of abundant micropores and the hysteresis loops at medium relative pressure demonstrate the existence of mesopores. Moreover, the rapid increase of the adsorption isotherms of DAC-700 and DAC-800 in the high pressure region (P/P_0 0.8−1) indicates the existence of macroporous structures. This result is consistent with the macroporous structure of DAC-700 and DAC-800 observed in the SEM images. From Table 1, DAC-700 has the largest specific surface area (1531 m^2/g) and pore volume (0.86 cm^2/g), and this structure can provide a high specific capacitance. Furthermore, from Figure 5B, DAC-700 also has a pore size distribution over a broad range. This hierarchical pore structure can enhance the rate performance and cycle stability of the DAC-700 electrode.

Electrochemical impedance spectroscopy (EIS) was used to evaluate the electrochemical performance of the samples, and the results are shown in Figure 6A. The x-axis intercept in the figure represents the equivalent series resistance (R_S).[32] The R_S values of DAC-600, DAC-700, and DAC-800 are 0.58, 0.56, and 0.49 Ω, respectively. The above data indicate that a higher carbonization temperature is conducive to the improvement of the electrical conductivity of activated carbon. R_{CT} is the charge transfer resistance of the electrode, and its value is fitted by Zview software according to the equivalent circuit (Figure 6A inset). The R_{CT} values of DAC-600, DAC-700, and DAC-800 are 0.59, 0.10, and 0.23 Ω, respectively. The R_{CT} of DAC-700 is obviously lower than that of DAC-600 and DAC-800, which is more beneficial to the energy storage of N, P-containing groups on the surface of DAC-700 electrode through chemical reaction.[33] In the low frequency region of the Nyquist plots, the curves of DAC-700 and DAC-800 were evidently steeper than that of DAC-600. This phenomenon indicated that the hierarchical pore structure of DAC-700 and DAC-800 is conducive to the migration of ions in the electrode, which lead to a relatively lower Warburg diffusion resistance (Z_w).[17,34,35]

The electrochemical properties of all DAC samples were studied by GCD test. As displayed in Figure 6B, compared with DAC-600 (102.2 F/g) and DAC-800 (126.0 F/g), DAC-700 electrode showed the largest specific capacitance (263.9 F/g) when the current density was 1 A/g. Moreover, the coulomb efficiencies of DAC-600, 700, and 800 are 97.8, 98.5, and 99.3%, respectively, indicating that the DAC-based electrode materials have excellent reversibility.

The main reasons for the optimal performance of DAC-700 are as follows: (1) DAC-700 has the highest specific surface area and a hierarchical pore structure. (2) Compared with DAC-800, DAC-700 has a higher doping content. These doped nitrogen and phosphorus atoms can not only contribute to the generation of pseudocapacitance, but also improve the wettability and conductivity of activated carbon materials. (3) Compared with DAC-600, DAC-700 has lower R_S, R_{CT}, and Z_w, which further improves its electrochemical performance for energy storage.

https://doi.org/10.1021/acsomega.2c04369
ACS Omega 2022, 7, 37564−37571

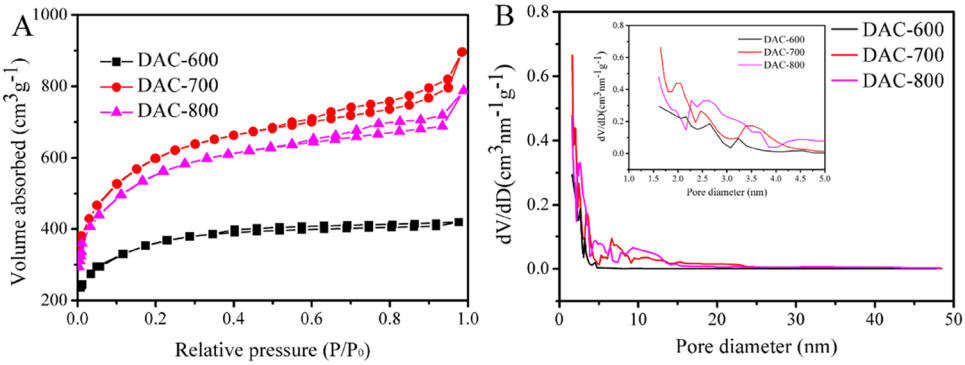

Figure 5. (A) Nitrogen adsorption/desorption isotherms and (B) pore size distributions of DAC samples.

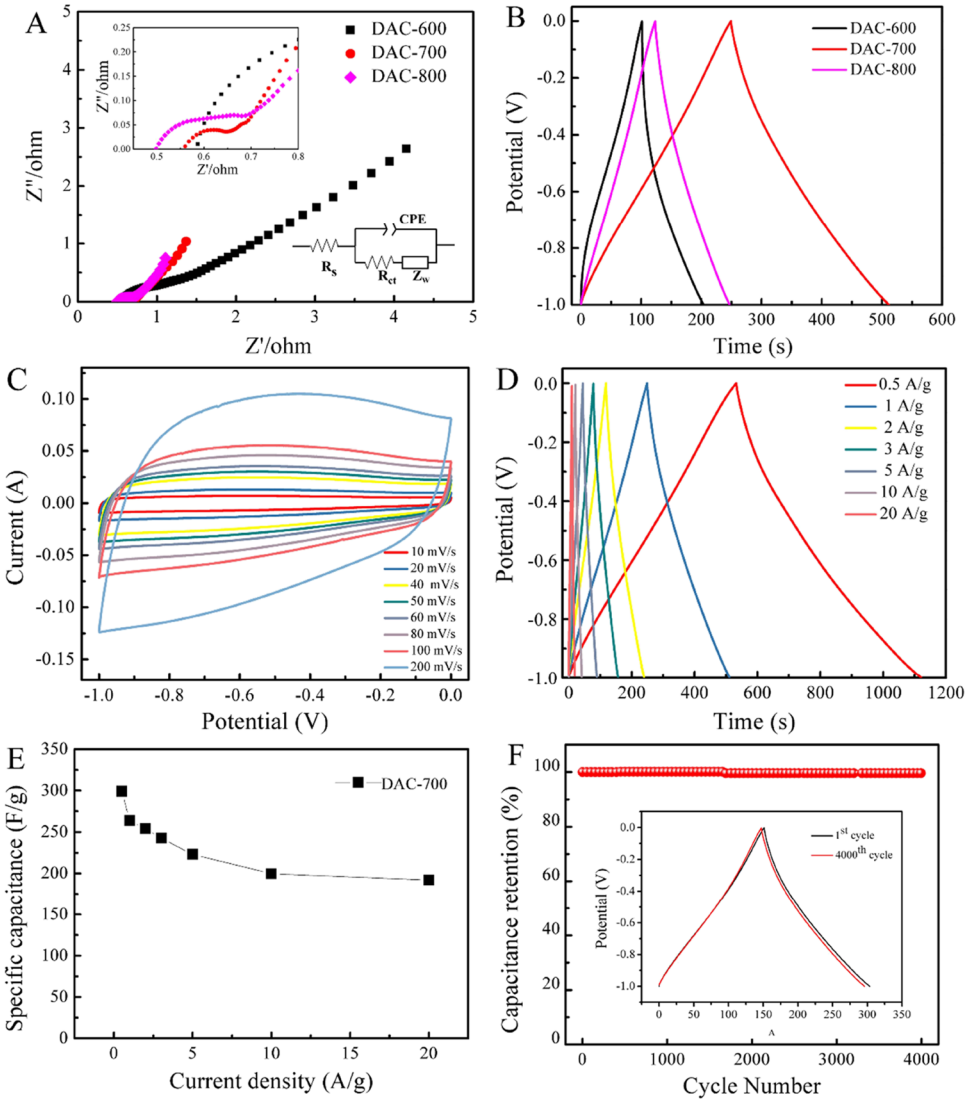

Figure 6. Electrochemical performance of DAC electrodes under a three-electrode system in 6 M KOH (A) Nyquist plots of all DAC electrodes (Inset: the corresponding equivalent circuit model). (B) GCD curves of all DAC electrodes at a current density of 1 A/g. (C) CV curves of DAC-700 electrode at various scan rates. (D) GCD curves of DAC-700 electrode at different current densities. (E) Specific capacitances as a function of current density. (F) Cycling performance of DAC-700 electrode at 1 A/g (Inset: CV profile of DAC-700 electrode for 1st and 4000th cycle).

Based on the above analysis, we mainly studied the performance of DAC-700 electrode in the subsequent experiments.

Figure 6C shows the CV curves of DAC-700 at different scan rates. It can be seen that the CV profiles present approximate rectangular shapes with indistinct redox peaks, suggesting that this electrode material has both electric double-layer capacitance and reversible pseudocapacitance caused by the heteroatom groups. To further investigate the electrochemical performance of DAC-700, GCD tests were performed at various current densities. As displayed in Figure 6D, the GCD curves of DAC-

https://doi.org/10.1021/acsomega.2c04369
ACS Omega 2022, 7, 37564−37571

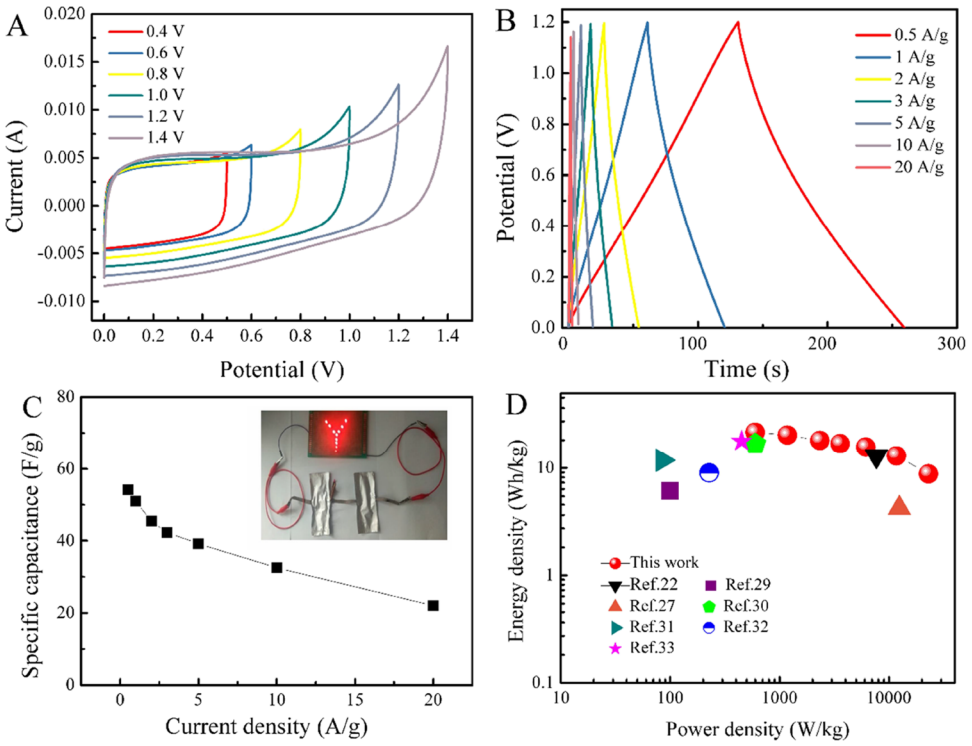

Figure 7. Electrochemical measurement results of the DAC-700//DAC-700 symmetric supercapacitor in 6 M KOH electrolyte. (A) CV curves in different voltage ranges at the scan rate of 10 mV/s. (B) GCD curves at various current densities. (C) Specific capacitances as a function of current density (Inset: the application of DAC-700//DAC-700 symmetric supercapacitor). (D)Ragone plots.

700 exhibited symmetric triangular-type profile with a negligible IR drop, indicating a low internal resistance. From Figure 6E, the specific capacitance (C_s) calculated from the GCD curves at a current density of 0.5 A/g is 299.1 F/g. It is worth noting that when the current density increased to 20 A/g, the specific capacitance still remained at 192.0 F/g. This excellent rate capability can be attributed to the low internal resistance of DAC-700 and the hierarchical porosity structure, which provides a fast diffusion rate of ions. As shown in Figure 6F, the capacitance retention of DAC-700 remained 99.6% after 4000 cycles at a current density of 1 A/g. This remarkable cycling stability can be mainly ascribed to the good structural stability and the highly reversible redox reaction on the surface of DAC-700.

In order to further explore the practical application performance of DAC-700 electrode, a symmetrical supercapacitor (DAC-700//DAC-700) was fabricated in which two identical HBC-700 electrodes were used as both the positive and negative electrodes and 6 M KOH solution was used as an electrolyte. CV measurement was carried out under different voltage ranges to determine the optimal potential window. As seen in Figure 7A, the curve remains approximately rectangular even in the voltage range of 0−1.2 V. However, a rapid current increase was observed when the voltage rose to 1.4 V. Therefore, a potential window of 0−1.2 V was determined for the following tests. As shown in Figure 7B, even at a high current density of 10 A/g, the GCD curve still presented a symmetrical and linear profile, which indicates that the DAC-700//DAC-700 has a low internal resistance and a well-developed hierarchical pore structure to accelerate the ion diffusion. From Figure 7C, the specific capacitance of DAC-700//DAC-700 was about 55.4 F/g at a current density of 0.5 A/g and the supercapacitor showed a good rate capability, as it retained more than 72.4% of the initial specific capacitance when the current density was increased to 5 A/g. The inset in Figure 7C shows that DAC-700//DAC-700 can easily light the LEDs, which further demonstrates its practical application performance. The Ragone plot of the symmetric supercapacitor is shown in Figure 7D. The DAC-700//DAC-700 achieved an excellent energy density of 21.6 Wh/kg at a power density of 598.2 W/kg, with the retention of 13.0 Wh/kg at a high power density of 11,700 W/kg. Moreover, the energy−power density characteristics of DAC-700//DAC-700 were found to be considerably higher than some other supercapacitors based on biomass-derived carbon.[26,31,36−40]

4. CONCLUSIONS

Activated carbon is one of the most widely used electrode materials for supercapacitors. In order to prepare activated carbon electrode with excellent performance and low cost, the flower of daylily was used as a precursor for the synthesis of activated carbon in this work. Through a simple carbonization and activation process, the nitrogen and phosphorus co-doped carbon material with a three-dimensional porous structure was prepared. High nitrogen and phosphorus contents can be obtained in the as-prepared samples, which can be attributed to the high content of protein and phospholipid molecules in daylily. The obtained electrode materials have a high specific capacitance (299.1 F/g at 0.5 A/g) and an excellent cycling stability with about 99.6% capacitance retention after 4000 cycles. The as-fabricated symmetrical supercapacitor exhibited a high specific capacitance of 55.4 F/g at a current density of 0.5 A/g and it also showed a good rate capability. Moreover, the as-fabricated symmetrical supercapacitor shows a good energy density and power density (21.6 Wh/kg at a power density of 598.2 W/kg), which is better than many other materials reported in the literature. These results indicate that the porous

https://doi.org/10.1021/acsomega.2c04369
ACS Omega 2022, 7, 37564−37571

carbon materials prepared by daylily have a good application prospect in the energy storage field.

■ ASSOCIATED CONTENT

Supporting Information

The Supporting Information is available free of charge at https://pubs.acs.org/doi/10.1021/acsomega.2c04369.

Preparation process of the two-electrode cell (PDF)

■ AUTHOR INFORMATION

Corresponding Authors

Tianxiang Jin − *Jiangxi Province Key Laboratory of Polymer Micro/Nano Manufacturing and Devices, East China University of Technology, Nanchang, Jiangxi 330013, China*; orcid.org/0000-0001-5950-6792; Email: 201660027@ecut.edu.cn

Chunyan Wang − *Jiangxi Province Key Laboratory of Polymer Micro/Nano Manufacturing and Devices, East China University of Technology, Nanchang, Jiangxi 330013, China*; Email: chunyanwang@ecut.edu.cn

Authors

Jingwei Su − *Jiangxi Province Key Laboratory of Polymer Micro/Nano Manufacturing and Devices, East China University of Technology, Nanchang, Jiangxi 330013, China*

Qingyun Luo − *Jiangxi Province Key Laboratory of Polymer Micro/Nano Manufacturing and Devices, East China University of Technology, Nanchang, Jiangxi 330013, China*

Wei Zhu − *Jiangxi Province Key Laboratory of Polymer Micro/Nano Manufacturing and Devices, East China University of Technology, Nanchang, Jiangxi 330013, China*

Haizhen Lai − *Jiangxi Province Key Laboratory of Polymer Micro/Nano Manufacturing and Devices, East China University of Technology, Nanchang, Jiangxi 330013, China*

Dejuan Huang − *Jiangxi Province Key Laboratory of Polymer Micro/Nano Manufacturing and Devices, East China University of Technology, Nanchang, Jiangxi 330013, China*

Complete contact information is available at: https://pubs.acs.org/10.1021/acsomega.2c04369

Notes

The authors declare no competing financial interest.

■ ACKNOWLEDGMENTS

The authors are grateful for the financial support of the Natural Science Foundation of Jiangxi (20212BAB214002), College Students' Innovative Entrepreneurial Training Plan Program (202210405016) and the National Natural Science Foundation of China (41361088, 41867063).

■ REFERENCES

(1) Panwar, N. L.; Kaushik, S. C.; Kothari, S. Role of renewable energy sources in environmental protection: A review. *Renew. Sustainable Energy Rev.* **2011**, *15*, 1513−1524.

(2) Ren, G.; Li, Y.; Chen, Q.; Qian, Y.; Zheng, J.; Zhu, Y.; Teng, C. Sepia-Derived N, P Co-doped Porous Carbon Spheres as Oxygen Reduction Reaction Electrocatalyst and Supercapacitor. *ACS Sustainable Chem. Eng.* **2018**, *6*, 16032−16038.

(3) Raghavendra, K. V. G.; Vinoth, R.; Zeb, K.; Muralee Gopi, C. V. V.; Sambasivam, S.; Kummara, M. R.; Obaidat, I. M.; Kim, H. J. An intuitive review of supercapacitors with recent progress and novel device applications. *J. Energy Storage* **2020**, *31*, No. 101652.

(4) Zhu, M.; Shao, Q.; Pi, Y.; Guo, J.; Huang, B.; Qian, Y.; Huang, X. Ultrathin Vein-Like Iridium−Tin Nanowires with Abundant Oxidized Tin as High-Performance Ethanol Oxidation Electrocatalysts. *Small* **2017**, *13*, No. 1701295.

(5) Ren, G.; Chen, Q.; Zheng, J.; Huang, B.; Qian, Y. N-doped carbon nanofibers aerogels derived from aramid as efficient electrocatalysts for oxygen reduction reaction in alkaline and acidic media. *J. Electroanal. Chem.* **2018**, *829*, 177−183.

(6) Zhu, T.; Ding, J.; Shao, Q.; Qian, Y.; Huang, X. P,Se-Codoped MoS2 Nanosheets as Accelerated Electrocatalysts for Hydrogen Evolution. *ChemCatChem* **2019**, *11*, 689−692.

(7) Borenstein, A.; Hanna, O.; Attias, R.; Luski, S.; Brousse, T.; Aurbach, D. Carbon-based composite materials for supercapacitor electrodes: a review. *J. Mater. Chem. A* **2017**, *5*, 12653−12672.

(8) Yan, J.; Wang, Q.; Wei, T.; Fan, Z. Recent Advances in Design and Fabrication of Electrochemical Supercapacitors with High Energy Densities. *Adv. Energy Mater.* **2014**, *4*, No. 1300816.

(9) Zhao, L.; Fan, L.-Z.; Zhou, M.-Q.; Guan, H.; Qiao, S.; Antonietti, M.; Titirici, M.-M. Nitrogen-Containing Hydrothermal Carbons with Superior Performance in Supercapacitors. *Adv. Mater.* **2010**, *22*, 5202−5206.

(10) Pandolfo, A. G.; Hollenkamp, A. F. Carbon properties and their role in supercapacitors. *J. Power Sources* **2006**, *157*, 11−27.

(11) Jing, X.; Wang, L.; Qu, K.; Li, R.; Kang, W.; Li, H.; Xiong, S. KOH Chemical-Activated Porous Carbon Sponges for Monolithic Supercapacitor Electrodes. *ACS Appl. Energy Mater.* **2021**, *4*, 6768−6776.

(12) Liu, L.; Niu, Z.; Chen, J. Flexible supercapacitors based on carbon nanotubes. *Chin. Chem. Lett.* **2018**, *29*, 571−581.

(13) Yu, X.; Li, N.; Zhang, S.; Liu, C.; Chen, L.; Xi, M.; Song, Y.; Ali, S.; Iqbal, O.; Han, M.; et al. Enhancing the energy storage capacity of graphene supercapacitors via solar heating. *J. Mater. Chem. A* **2022**, *10*, 3382−3392.

(14) Wang, C.; Bai, L.; Zhao, F.; Bai, L. Activated carbon fibers derived from natural cattail fibers for supercapacitors. *Carbon Lett.* **2022**, *32*, 907−915.

(15) Wang, L.; Huang, M.; Huang, J.; Tang, X.; Li, L.; Peng, M.; Zhang, K.; Hu, T.; Yuan, K.; Chen, Y. Coupling of EDLC and the reversible redox reaction: oxygen functionalized porous carbon nanosheets for zinc-ion hybrid supercapacitors. *J. Mater. Chem. A* **2021**, *9*, 15404−15414.

(16) Wang, T.; He, X.; Gong, W.; Kou, Z.; Yao, Y.; Fulbright, S.; Reardon, K. F.; Fan, M. Three-dimensional, heteroatom-enriched, porous carbon nanofiber flexible paper for free-standing supercapacitor electrode materials derived from microalgae oil. *Fuel Process. Technol.* **2022**, *225*, No. 107055.

(17) Chen, J.; Lin, C.; Zhang, M.; Jin, T.; Qian, Y. Constructing Nitrogen, Selenium Co-Doped Graphene Aerogel Electrode Materials for Synergistically Enhanced Capacitive Performance. *ChemElectroChem* **2020**, *7*, 3311−3318.

(18) Huang, B.; Wu, Y.; Chen, B.; Qian, Y.; Zhou, N.; Li, N. Transition-metal-atom-pairs deposited on g-CN monolayer for nitrogen reduction reaction: Density functional theory calculations. *Chin. J. Catal.* **2021**, *42*, 1160−1167.

(19) Liu, X.; Zhou, Y.; Wang, C.-L.; Liu, Y.; Tao, D.-J. Solvent-free self-assembly synthesis of N-doped ordered mesoporous carbons as effective and bifunctional materials for CO2 capture and oxygen reduction reaction. *Chem. Eng. J.* **2022**, *427*, No. 130878.

(20) Chen, W.-T.; Han, S.; Gao, Z.-T.; Sun, M.-S.; Li, Z.-M.; Tao, D.-J. B/N co-doped carbon supported molybdenum carbide catalysts with oxygen vacancies for facile synthesis of flavones through oxidative dehydrogenation. *J. Colloid Interface Sci.* **2022**, *623*, 735−743.

(21) Leng, J.; Luo, J.; Song, C.; Zhou, Y.; Li, Z.; Tao, D. Preparation of Co-N-C catalysts and "one-pot method" for synthesis of N-benzyl aniline. *CIESC J.* **2020**, *71*, 5016−5024.

(22) Gopalakrishnan, A.; Badhulika, S. Effect of self-doped heteroatoms on the performance of biomass-derived carbon for supercapacitor applications. *J. Power Sources* **2020**, *480*, No. 228830.

(23) Zhang, Z.; Tang, S.; Lin, X.; Liu, C.; Hu, S.; Huang, Q. N, P-doped multiphase transition metal sulfides are used for efficient

electrocatalytic oxygen evolution reaction. *Appl. Surf. Sci.* **2022**, *584*, No. 152546.
(24) Saini, S.; Chand, P.; Joshi, A. Biomass derived carbon for supercapacitor applications: Review. *J. Energy Storage* **2021**, *39*, No. 102646.
(25) Kim, M.; Puthiaraj, P.; Qian, Y.; Kim, Y.; Jang, S.; Hwang, S.; Na, E.; Ahn, W.-S.; Shim, S. E. High performance carbon supercapacitor electrodes derived from a triazine-based covalent organic polymer with regular porosity. *Electrochim. Acta* **2018**, *284*, 98−107.
(26) Wan, L.; Li, X.; Li, N.; Xie, M.; Du, C.; Zhang, Y.; Chen, J. Multi-heteroatom-doped hierarchical porous carbon derived from chestnut shell with superior performance in supercapacitors. *J. Alloys Compd.* **2019**, *790*, 760−771.
(27) Lei, S.; Chen, L.; Zhou, W.; Deng, P.; Liu, Y.; Fei, L.; Lu, W.; Xiao, Y.; Cheng, B. Tetra-heteroatom self-doped carbon nanosheets derived from silkworm excrement for high-performance supercapacitors. *J. Power Sources* **2018**, *379*, 74−83.
(28) Tan, Y.; Xu, C.; Chen, G.; Liu, Z.; Ma, M.; Xie, Q.; Zheng, N.; Yao, S. Synthesis of Ultrathin Nitrogen-Doped Graphitic Carbon Nanocages as Advanced Electrode Materials for Supercapacitor. *ACS Appl. Mater. Interface* **2013**, *5*, 2241−2248.
(29) Yan, X.; Yu, Y.; Ryu, S.-K.; Lan, J.; Jia, X.; Yang, X. Simple and scalable synthesis of phosphorus and nitrogen enriched porous carbons with high volumetric capacitance. *Electrochim. Acta* **2014**, *136*, 466−472.
(30) Wu, S.; Feng, C.; Fan, B.; Li, Y.; Wang, H.; Zhou, Y. N/O/P co-doped hierarchical porous graphitic carbon materials for high-rate supercapacitors. *J.Alloys Compd.* **2022**, *899*, No. 163282.
(31) Nanaji, K.; Upadhyayula, V.; Rao, T. N.; Anandan, S. Robust, Environmentally Benign Synthesis of Nanoporous Graphene Sheets from Biowaste for Ultrafast Supercapacitor Application. *ACS Sustainable Chem. Eng.* **2019**, *7*, 2516−2529.
(32) Wang, K.; Li, L.; Zhang, T.; Liu, Z. Nitrogen-doped graphene for supercapacitor with long-term electrochemical stability. *Energy* **2014**, *70*, 612−617.
(33) Cao, L.; Li, H.; Xu, Z.; Gao, R.; Wang, S.; Zhang, G.; Jiang, S.; Xu, W.; Hou, H. Camellia Pollen-Derived Carbon with Controllable N Content for High-Performance Supercapacitors by Ammonium Chloride Activation and Dual N-Doping. *ChemNanoMat* **2021**, *7*, 34−43.
(34) Jin, T.; Chen, J.; Wang, C.; Qian, Y.; Lu, L. Facile synthesis of fluorine-doped graphene aerogel with rich semi-ionic C−F bonds for high-performance supercapacitor application. *J. Mater. Sci.* **2020**, *55*, 12103−12113.
(35) Zhang, F.; Liu, H.; Wu, Z.; Zhang, J.; Cui, E.; Yue, L.; Hou, G. Polyacrylamide Gel-Derived Nitrogen-Doped Carbon Foam Yields High Performance in Supercapacitor Electrodes. *ACS Appl. Energy Mater.* **2021**, *4*, 6719−6729.
(36) Li, D.; Guo, Y.; Li, Y.; Liu, Z.; Chen, Z. Waste-biomass tar functionalized carbon spheres with N/P Co-doping and hierarchical pores as sustainable low-cost energy storage materials. *Renew. Energy* **2022**, *188*, 61−69.
(37) Chen, H.; Yu, F.; Wang, G.; Chen, L.; Dai, B.; Peng, S. Nitrogen and Sulfur Self-Doped Activated Carbon Directly Derived from Elm Flower for High-Performance Supercapacitors. *ACS Omega* **2018**, *3*, 4724−4732.
(38) Wang, J.; Shen, L.; Xu, Y.; Dou, H.; Zhang, X. Lamellar-structured biomass-derived phosphorus- and nitrogen-co-doped porous carbon for high-performance supercapacitors. *New J. Chem.* **2015**, *39*, 9497−9503.
(39) Jia, H.; Sun, J.; Xie, X.; Yin, K.; Sun, L. Cicada slough-derived heteroatom incorporated porous carbon for supercapacitor: Ultra-high gravimetric capacitance. *Carbon* **2019**, *143*, 309−317.
(40) Wu, D.; Cheng, J.; Wang, T.; Liu, P.; Yang, L.; Jia, D. A Novel Porous N- and S-Self-Doped Carbon Derived from Chinese Rice Wine Lees as High-Performance Electrode Materials in a Supercapacitor. *ACS Sustainable Chem. Eng.* **2019**, *7*, 12138−12147.

https://doi.org/10.1021/acsomega.2c04369
ACS Omega 2022, 7, 37564−37571